JOURNAL OF MATERIALS SCIENCE 33 (1998) 2639–2651

Structure characterization of a laser-processed Al–Mo alloy

Y. Y. QIU, A. ALMEIDA, R. VILAR
Departamento de Engenharia de Materiais, Instituto Superior Técnico, Av. Rovisco, Pais, 1096 Lisboa, Portugal
E-mail: i006@alfa.ist.utl.pt.

The surface structure of a laser-processed Al–Mo alloy has been characterized using scanning electron microscopy (SEM), transmission electron microscopy (TEM) and X-ray diffractory (XRD). The alloy was prepared by first laser alloying a mixture of Al and Mo powders into an Al substrate and then laser remelting the alloyed surface. Following the first laser alloying process, the needle-like equilibrium phases (Al_5Mo(h) and Al_5Mo(r)) are formed with a broad size ranges and distribute inhomogeneously in the α-Al solid solution matrix. This coarse structure is replaced by a finer, uniform dispersion of dendrites after the subsequent laser remelting. Four basic types of solid states precipitates are observed: (1) irregularly shaped particles constructing the dendrites and having a nearly Al_5Mo stoichiometry; (2) needle-like particles which is the Al_5Mo (r) phase; (3) Faceted particles having a cubic structure with a stoichiometry close to Al_7Mo; (4) tiny, equi-axed particles, with a rather narrow particle size distribution and a cubic structure.

1. Introduction

There is currently a great interest in improving the high temperature strength and wear resistance of Al alloys. To achieve this requirement, the alloy must be dispersion hardened with precipitates that do not coalesce significantly during long-term exposure to temperatures within the range 100–300°C. Al_xM_y (M = transition metal) intermetallic compound particles suit well the requirements for long-term dispersion strengthening [1–4]. Because transition metals present low diffusivity in Al, the materials formed of Al_xM_y particles dispersed in an α-Al solid solution matrix are inherently temperature resistant. However, to achieve the degree of dispersion needed, special techniques such as mechanical alloying, melt-spinning, and laser processing must be used. Among these techniques, laser surface alloying (LSA) has tremendous potential to achieve the required wear resistance, since it allows to obtain extremely fine dispersions of intermetallic compounds. When the treatment is carried out properly, intense convection ensures good homogenization of the melt and rapid solidification leads to fine-grained new materials with novel structures and interesting properties [5–7].

The development of a dispersion strengthened surface layer by LSA of Al alloys with Cr, Ni, Si, Fe and the resultant improvement in their surface properties have been reported in several studies [7–13]. However, the Al–Mo system received much less attentions in this aspect. The research on the Al–Mo were limited on extending the solid solubility by rapid solidification processing (RSP) [14] and on the precipitation behaviour, phase structure and thermal stability [15]. The equilibrium solid solubility of Mo in Al is very low ~0.07 at % Mo. Under conditions of rapid solidification, potential exists for suppressing wholly or partially the formation of the pro-peritectic constituent and thus extending usefully the concentration of Mo retained in metastable solid solution. Polesya *et al.* [16] reported that it is possible to retain about 2.5 at % Mo in solution in Al by melt spinning. However, after subsequent annealing, the solute atoms Mo are transported to the grain boundaries by pipe diffusion, and the only precipitation that is seen is at the boundaries, which precludes the possibility of age hardening of such alloy [17–18]. It has also reported that the presence of a very low Fe content in the alloys can lead to precipitation of very fine, dispersed quasicrystals within grain centres, together with the equilibrium phases $Al_{12}Mo$ at the grain boundaries [15, 19, 20].

The Al–Mo system is one of a group of Al-based, peritectic systems, such as the Al–Cr system which shows considerable potential for the development of a dispersion–strengthen surface layer by LCA [5–6]. Because the equilibrium solid solubility and the diffusivity of Mo in Al are very low, the possibility then exists also for production of fine dispersion of stable or metastable intermetallic phases by laser processing, which has lower solidification rate than that by melt-spinning.

Previous work [5] has found that hard and corrosion resistant surfaces can be produced on Al by laser alloying Mo powder with the Al substrate. The hardness of the surface layers can reach to 350 H_V and the refinement of the surface is achieved by the

subsequent laser remelting the alloyed surface. The previous work pertains mostly on the surface properties as function of the laser-processing parameters. Therefore, the present investigation is focused on the fine-scale characterization of the solidification microstructure, the identification of the phases, and the microchemical features. Transmission electron microscopy (TEM) is used for such purpose. TEM provides the best opportunity for microstructure and crystal structure characterization of laser processed materials since it has very small probe size (from 3.5 nm to 20 nm) which makes it possible to work always with single crystals and it can be operated at diffraction mode and image mode. In addition, TEM energy dispersive X-ray spectroscopy (EDS) provides useful information about the microchemistry.

2. Experimental procedure

Laser processing was performed in two steps: first, laser surface alloying (LSA) the Al–Mo ($\sim$8.6 at %) powder mixture (the diameters of the Al and Mo powder particles were 150 mm and 71 mm, respectively) into pure Al substrate, and second, laser surface remelting (LSR) the alloyed surface. LSA was carried out by the blown power technique using a 3 kW CO_2 laser. The power density and the interaction time varied in the ranges ($1.1–2.6 \times 10^5$ W cm^{-2} and 0.04–0.3 s). The alloying treatments were carried out with a powder flow rate of 0.03 g s^{-1}. The Al substrate was previously cleaned by sand blasting. To reduce the absorbed moisture, the Al and the Mo powder mixtures were dried in an oven at 70°C for 3 h just before the experiments. A 50% overlap between consecutive tracks was used to obtain a melted layer with a uniform depth. Oxidation of the melted pool was reduced by blowing Ar over the surface of the samples during the laser treatment. LSR was performed by remelting the laser alloyed layers in a direction normal to the direction previously used for LSA. The scanning speed used for LSR was 20 mm s^{-1} under the laser power of 2 kW.

The microstructures were characterized using a S-2400 scanning electron microscope (SEM) operated at 25 kV and a H-8100 TEM operated at 200 kV. The samples for SEM were first metallographically prepared and then etched with Kelley's reagent. Thin foils for TEM investigation were prepared by a twin jet-electropolishing technique using a solution of 5% $HClO_4$ in methanol at 10 V and at temperature of -30°C. The X-ray diffraction (XRD) and selected-area electron diffraction techniques (SAD) were used for the identification of the phases. The morphologies of the intermetallics were observed through the bright-field (BF) and dark-field (DF) imaging conditions. The bulk composition of the sample was determined by electron probe microanalysis (EPMA). The compositions of the individual intermetallics were checked by means of electron beam microanalysis using an energy dispersive X-ray spectrometer (EDS), which is attached to the TEM. A nanoprobe model with probe size $\sim$5 nm was used for the EDS analysis. A standardless quantitative analysis program based on the Cliff–Lorimer data analysis algorithm was used to obtain the quantitative compositions from EDS data.

3. Results

3.1. SEM and XRD analysis

Chemical analysis by EPMA indicates that the studied Al–Mo alloy surface contains an average of 1.5 at % Mo after the two-step laser processing. A transverse cross-section of this alloy is shown in Fig. 1, where two distinct microstructure zones were detectable. The zone near the bottom corresponds to the material that was not affected by laser remelting (alloyed layer, A). The solidification structure comprises the α-Al solid solution with the needle-like particles and a few small dendrites. These particles have a broad size distribution and distributed inhomogeneously. The faceted plate-like particles are also found which are precipitated mostly near the top of the alloyed layer. Some pores and undissolved Mo particles are observed too.

The zone close to the free surface experienced both laser alloying and laser remelting (remelted layer, R) and have a finer, dendrite solidification structure (Fig. 1). Those needle-like particles from the alloyed layer also appeared in the remelted layer. These particles either aggregate at some regions or distribute between the dendrites (Fig. 2). The undissolved Mo particles are completely diminished.

Fig. 3 shows the two XRD profiles obtained from the alloyed layer (Fig. 3a) and the remelted layer (Fig. 3b). The Al solid solution peaks have been identified and are indicated in the profile. Both profiles are analysed by comparing them with all the reported phases in Al–Mo binary systems based on the peaks position and the relative intensity values. Table I lists the analysis results.

Table I indicates that both Al_5Mo (h) and Al_5Mo (r) phases can be found in the profile shown in Fig. 3a. However, only Al_5Mo (r) phase is found to match the profile shown in Fig. 3b perfectly if this profile is shifted to the left a little bit and this movement is corresponding to that each of the measured 2θ° minus 0.05°. The 0.05° error is within the range of the

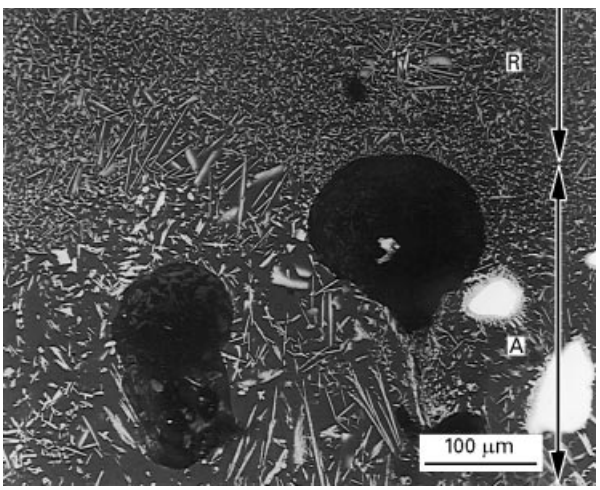

Figure 1 SEM image of the cross-section of the Al–Mo alloy prepared by laser alloying and remelting processes.

possible shift of the measured X-ray profile (the difference of the $2\theta^{\circ}$ value between the same Al matrix peaks in two profiles is 0.05°). It can be concluded that, in the alloyed layer, the Al_5Mo (h) and Al_5Mo (r) phases coexist. In the remelted layer, Al_5Mo (r) phase was found to be the major phase. The unidentified peaks indicates the existence of new phases.

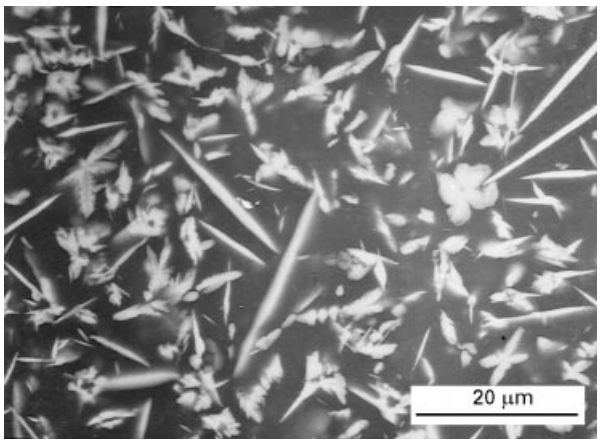

Figure 2 Solidification structure on the surface of Al–Mo alloy prepared by laser alloying and remelting processes.

3.2. TEM analysis

The TEM studies involving selected area diffraction (SAD) and microanalysis (EDS) were carried out with a view to gaining an understanding of the finer structural details arising in the laser processing. The sample analysed covers mainly the remelted layer. Four kinds of particles with different morphologies are observed: (1) a relatively large fraction of needle-like particles; (2) a large fraction of the dendrites, (3) a small fraction of faceted particles some of which are located at the centre of the dendrites; (4) tiny, equi-axed particles, with round 20 nm in diameter, and distributed along the Al cell boundary.

The needle-like particles have a composition of 83.3 ± 1.7 at % Al and 16.7 ± 1.7 at % Mo which gives an Al_5Mo stoichiometry, according to EDS analysis. Fig. 4 shows one typical EDS profile measured from these particles. Some of these particles show periodically spaced faulted dipoles parallel to foil

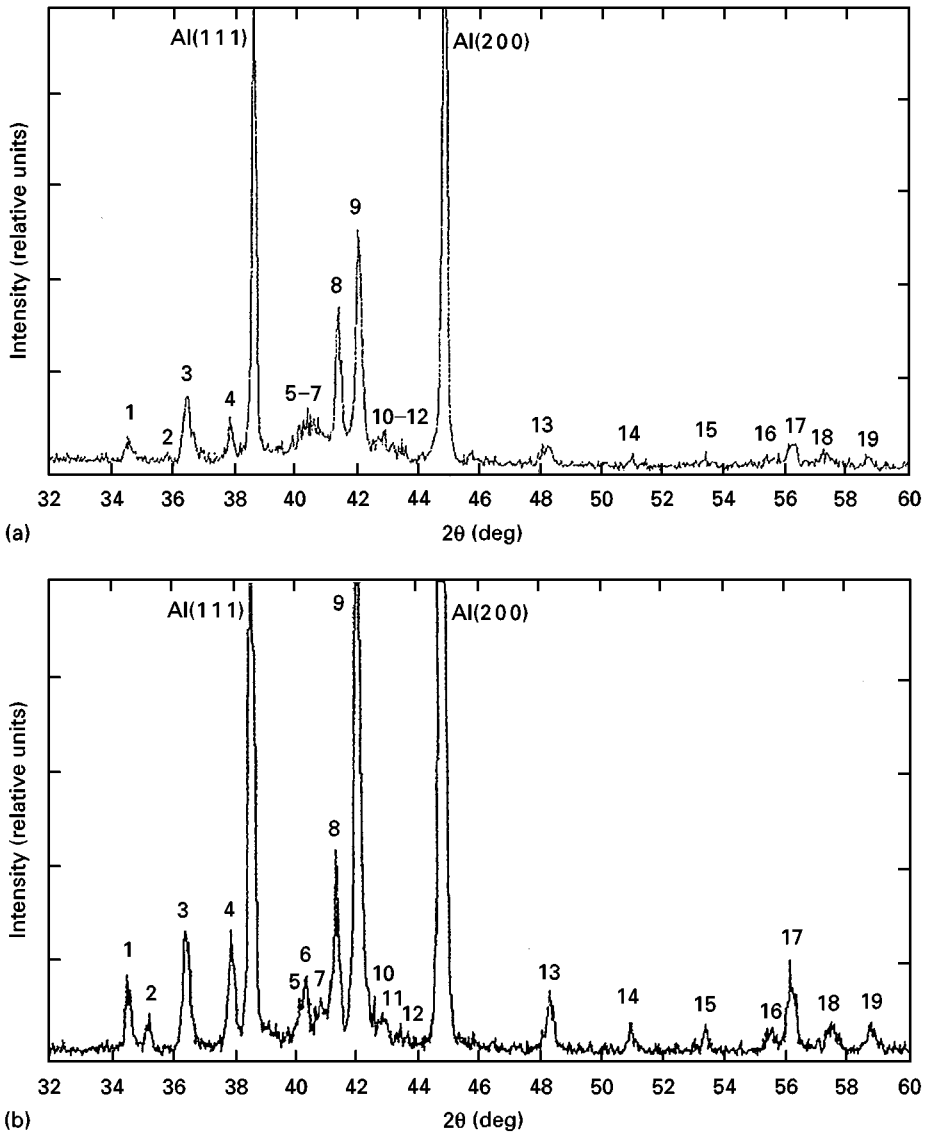

Figure 3 XRD profiles taken from (a) alloyed layer and (b) remelted layer of the Al–Mo alloy prepared by laser alloying and remelting processes.

TABLE I Proposed phase identification for XRD profiles of Fig. 3

	Result from profile (a)		Result from profile (b)	
No.	2(θ°)	Phases proposed with {2(θ°), relative intensity value} (corresponding plane indexes)	2(θ°)	Phases proposed with {(2θ°), relative intensity value} (corresponding plane indexes)
1	34.51	Al_5Mo(r) {34.4, 11.1}(10 − 8)	34.51	same as (a)
	34.61	?	34.61	?
	34.8	?		
2	35.2	?	35.2	?
	35.8	?		
3	36.56	Al_5Mo(h) {36.56, 26.3}(2 − 10)	36.4	Al_5Mo(r) {36.26, 27.8}(2 − 10)
	36.47	?	36.6	?
	36.3	Al_5Mo(r) {36.26, 27.8}(2 − 10)		
4	37.99	Al_5Mo(h) {37.99, 18.5}(2 − 11)	37.82	Al_5Mo(r) {37.74, 10.3}(2 − 1 − 3)
	37.86	?	37.9	?
	37.74	Al_5Mo(r) {37.74, 10.3}(2 − 1 − 3)	40.1	?
5	40.2	Al_5Mo(r) {40.27, 6.8} (1010)	40.3	Al_5Mo(r) {40.27, 6.8} (1010)
6	40.5	?	40.5	?
7	40.8	Al_5Mo(h) {40.7, 27.2}(004)	40.8	?
			40.7	?
			41	?
8	41.4	Al_5Mo(r) {41.27, 25.5} (0012)	41.36	Al_5Mo(r) {41.27, 25.5} (0012)
9	42.06	Al_5Mo(h) {42.03, 100}(2 − 12)	42.02	Al_5Mo(r) {41.9, 100}(2 − 16)
	41.9	Al_5Mo(r) {41.9, 100}(2 − 16)		
10	42.5	Al_5Mo(h) {42.46, 1.6}(200)	42.5	?
11	42.9	Al_5Mo(r) {42.7, 5.6}(202)	42.8	Al_5Mo(r) {42.7, 5.6}(202)
12	43.5	Al_5Mo(h) {43.73, 8.9}(201)	43.4	?
13	48.1 ~	Al_5Mo(h) {48.15, 8.3}(2 − 13)	48.3	Al_5Mo(r) {48.19, 4.5}(2 − 19)
	48.3	Al_5Mo(r) {48.19, 4.5}(2 − 19)	48.4	?
14	51	Al_5Mo(r) {50.84, 3.0}(208)	51	Al_5Mo(r) {50.84, 3.0}(208)
15	53.01	Al_5Mo(h) {53.01, 4.5}(203)	53.4	Al_5Mo(r) {53.32, 2.5}(10 − 14)
	53.45	Al_5Mo(r) {53.32, 2.5}(10 − 14)		
16	55.8	Al_5Mo(h) {55.85, 12.1}(2 − 14)	55.4	Al_5Mo(r) {55.3, 2.2}(20 − 10)
			55.6	?
17	56.25	Al_5Mo(r) {56.08, 12.3}(2 − 112)	56.16	Al_5Mo(r) {56.08, 12.3}(2 − 112)
18	57.25	Al_5Mo(h) {57.25, 1.1}(3 − 10)	57.3	Al_5Mo(r) {57.23, 3.9}(3 − 1 − 2)
	57.4	Al_5Mo(r) {57.23, 3.9}(3 − 1 − 2)	57.5	?
19	58.3	Al_5Mo(h) {58.27, 6.2}(3 − 11)	58.7	Al_5Mo(r) {58.63, 3.5}(3 − 14)
	58.7	Al_5Mo(r) {58.63, 3.5}(3 − 14)	58.9	?

Note: "Al_5Mo(h) {36.56, 26.3}(2 − 10)" signifies Al_5Mo(h) phase; {2(θ°) = 36.56; relative intensity value = 26.3}; (corresponding plane indexes) = (2, −1, 0).

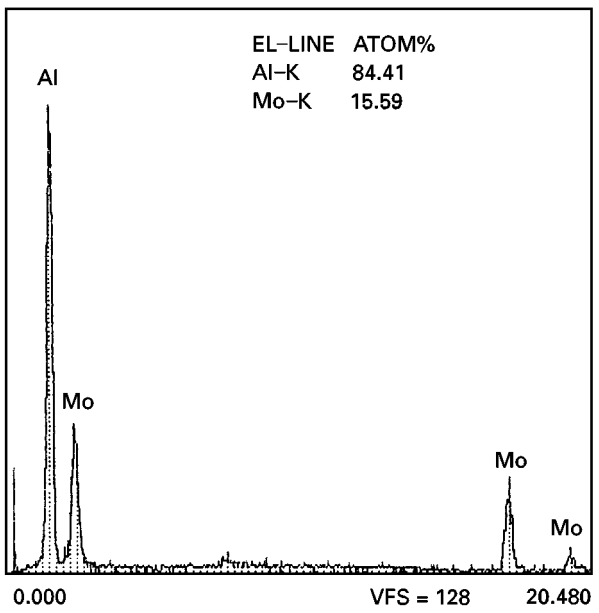

Figure 4 A typical EDS-profile measured from the needle-like particles from Al–Mo alloy prepared by laser alloying and remelting processes.

surface (Fig. 5a). These particles are identified to be Al_5Mo (r) phase as that reported by Schuster and Ipser [21]. The corresponding SAD patterns with zone axis [1, 0, −1, 1], [1, 0, −1, 0], and [2, 1, −3, 0] are shown in Fig. 5b, c, and d, respectively. The extra reflection in Fig. 5d (see arrow) is from the double reflections.

The isolated faceted particles shown in Fig. 6a and b have an average composition of 87.1 ± 0.6 at % Al and 12.9 ± 0.4 at % Mo and this composition is close to Al_7Mo stoichiometry. The extensive SAD pattern analysis indicated that this phase has a Fm3m structure with the lattice parameter round 1.45 nm which do not match to any of the reported phases in Al–Mo system. The SAD patterns with zone axis [0 1 1], [0 1 3], [0 1 2], and [1 1 2] from these particles are shown in Fig. 6c, d, e, f, respectively. One typical EDS profile from these particles is shown in Fig. 7. These faceted particles are found with rather low fraction in the remelted layer.

TEM examination of the dendrites in three different areas are presented in Fig. 8. The dendrites with the sizes range from 5 μm to 22 μm homogeneously distributed in a cellular-dendritic matrix of α-Al. The tiny equi-axed particles (~20 nm) with narrow size

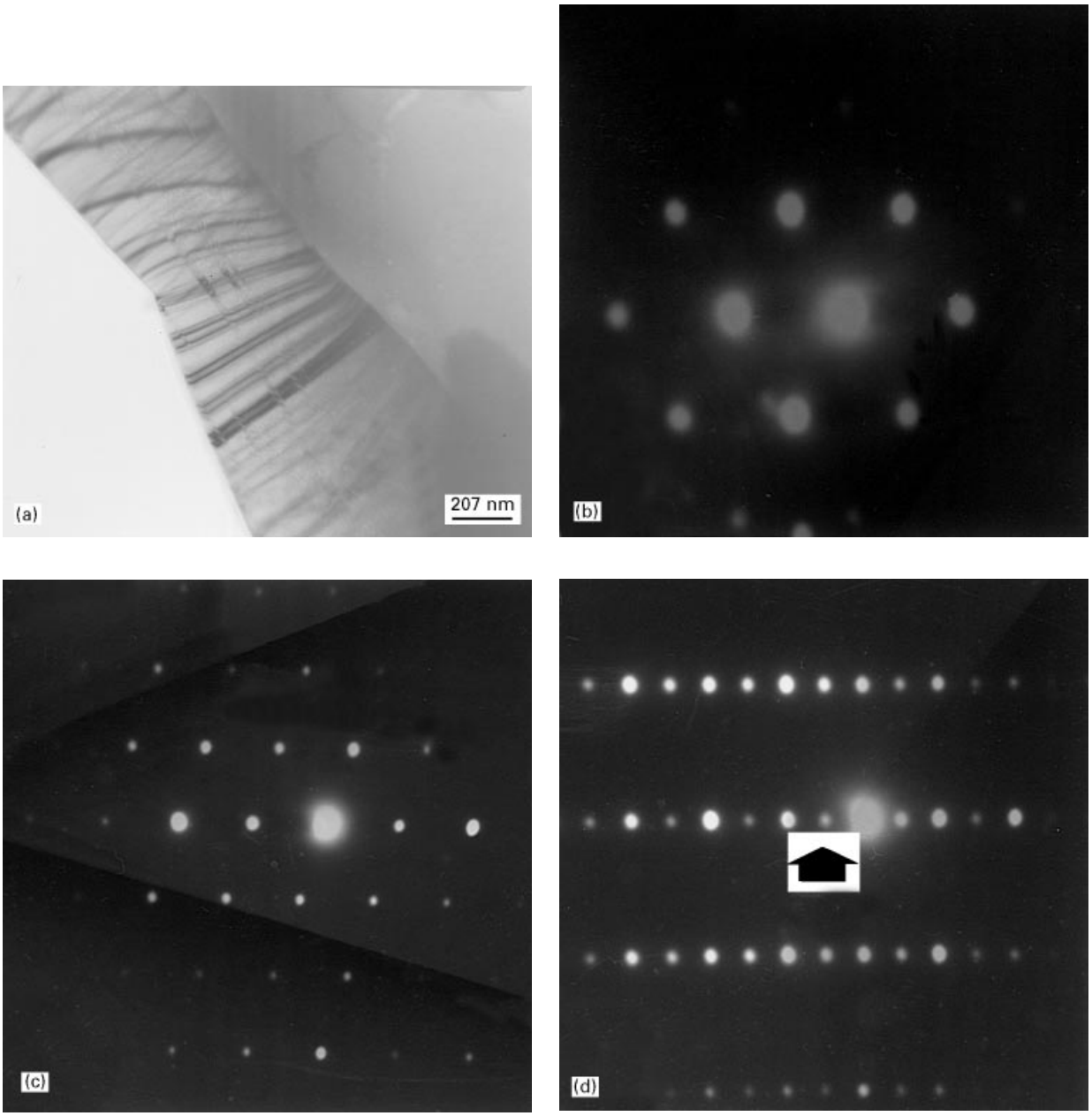

Figure 5 (a) TEM bright-field image of an needle-like particle from Al–Mo alloy prepared by laser alloying and remelting processes. The associated SAD patterns with different zone axes shown in: (b) [1, 0, −1, 1]; (c) [1, 0, −1, 0]; and (d) [2, 1, −3, 0].

distribution precipitated along the α-Al cellular boundary. These small particles have a similar structure as those of faceted particles but with a lattice parameter round 1.9 nm based on SAD analysis.

The dendrites were observed in two main morphological forms. One form is shown in Fig. 9. These dendrites have a nearly 90° angle between their primary dendrite arms while the side branches have a nearly 45° angle with the primary dendrite arms (named as 90° dendrites). The primary dendrite arms do not develop at the same speed. Some arms grow a little fast and the small side branches are only found in some of the primary arms. It is noted that the dendrite arm that parallel to the Al cell boundary grows slightly fast than other directions. The extensive SAD pattern analysis for these dendrites indicates that these dendrites are not any of the phases reported for the Al–Mo system. It has a complicated tetragonal structure ($I/4\,mmm$, $a = 9.4$, $c = 6.0$). Fig. 10 shows several corresponding SAD patterns. A complete structure identification is still under study.

The other form of the dendrites is shown in Fig. 11. It is shown that the dendrites have only one preferred growing direction. They are also slightly branched and the side branches have a nearly 30° or 60° angles with the primary dendrite arms (named as 30° dendrites). It can be predicted that the small dendrite in Fig. 11d had five primary arms previously and one of the five arms disappeared during the growth of the dendrite. This phenomenon can be further confirmed by observing few dendrites, as shown in Fig. 12. These dendrites having five (Fig. 12a) and six dendrite arms (Fig. 12c) with mixed 90° and 60° angle between their primary arms. It is therefore assumed that the particles in Fig. 12a and c are the transition states between the dendrites shown in Fig. 9 and in Fig. 11. The 90° arms are not stable and they will disappear during the

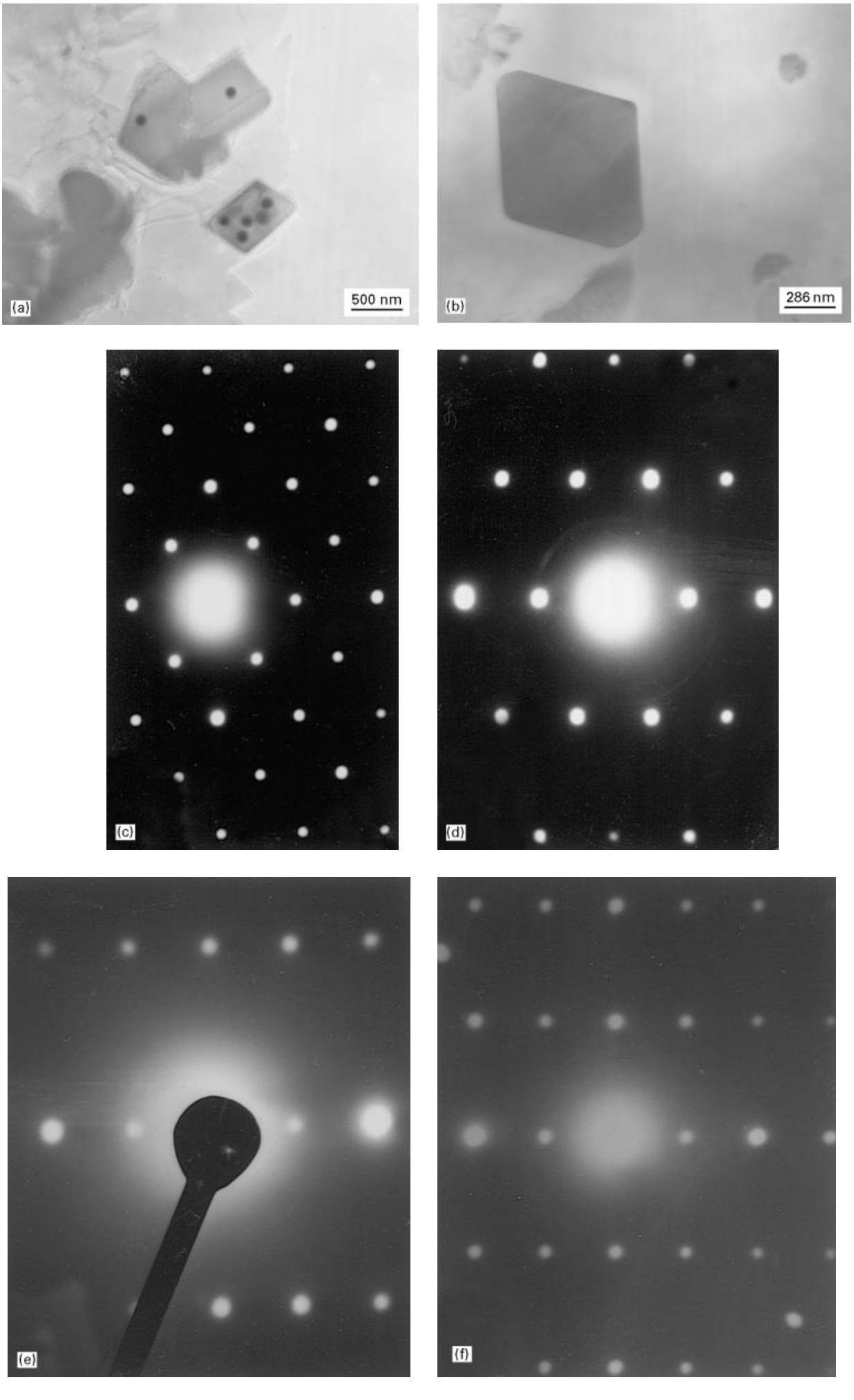
(a)
500 nm
(b)
286 nm
(c)
(d)
(e)
(f)

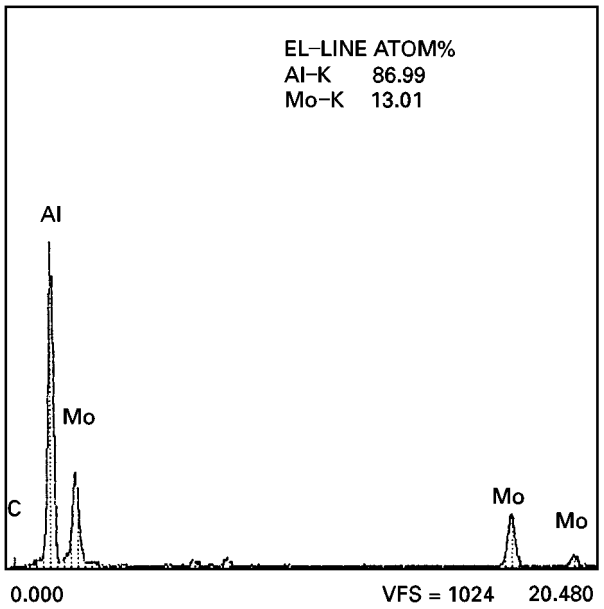

Figure 7 A typical EDS profile measured from the faceted particles in from Al–Mo alloy prepared by laser alloying and remelting processes.

dendrite growth. For example, the dendrite in Fig. 12a can change to that in Fig. 12b. The dendrite in Fig. 12c can change to Fig. 11a.

The SAD analysis for the dendrites in Fig. 11 indicates that they have a monoclinic stricture. Fig. 13 shows their SAD patterns and the corresponding computer simulations from a presumed structure (Cm, $a = b = 9.6$, $c = 9.5$, $\beta = 105^{\circ}$). EDS measurements have been performed on many of dendrites and it states that both dendrites have an average composition of 83.1 ± 1.8 at % Al and 16.9 ± 1.9 at % Mo. This result matches Al_5Mo stoichiometry.

As mentioned previously, some faceted particles are located at the centre of the dendrites (Fig. 14). The EDS analysis on these particles indicates that some of them have Al_5Mo stoichiometry as shown in Fig. 14c and some of them have rather lower Mo contents. It is not able to define the phase structure since the difficulties to perform SAD analysis on these particles. The EDS analysis found that the average Mo content in the matrix is around 0.9 ± 0.3 at %.

4. Discussion

As shown in the experimental section, laser surface alloying modifies the chemical composition of the radiated material, through application of pre-established quantities of alloying powders melted together with the basic material on its surface. Hence, an inhomogeneous composition on the surface is expected because of the incomplete mixing of the elements during the laser treatment. As a result, a rather coarse solidification structure formed (see the alloyed layer in Fig. 1). The precipitated intermetallics have a broad size range and distribute inhomogeneously in

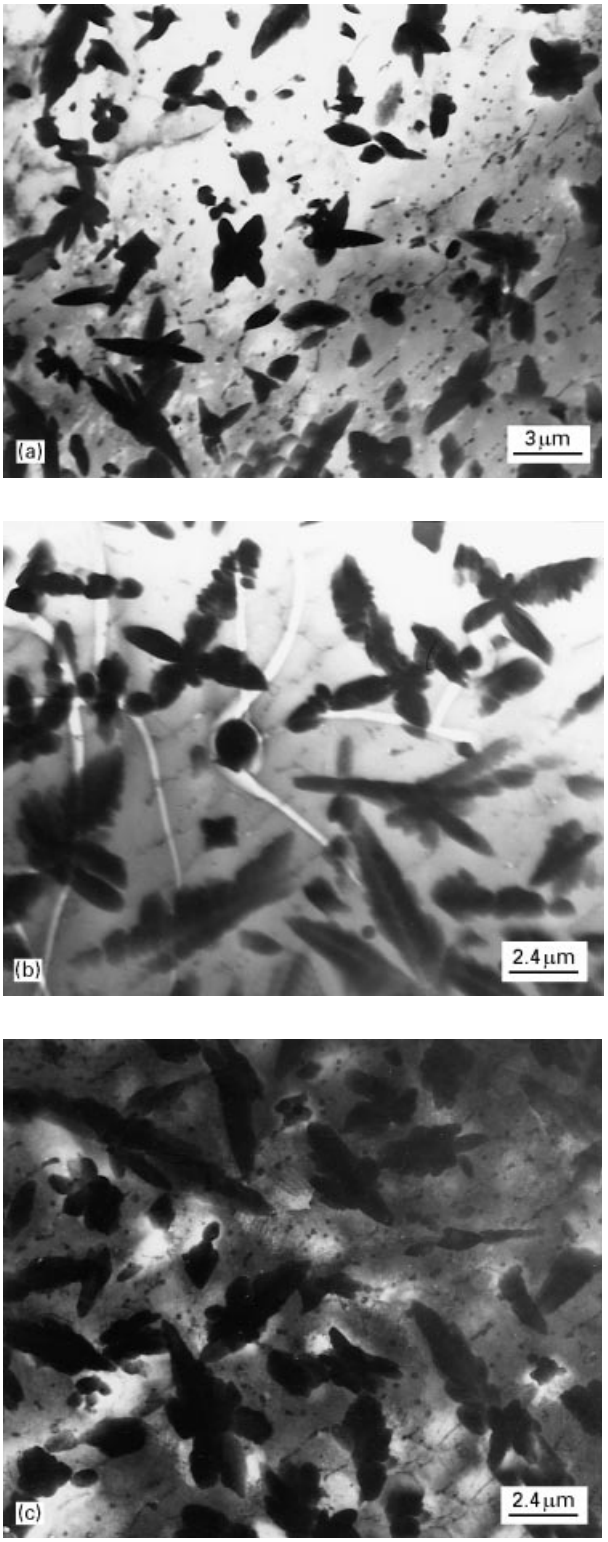

Figure 8 TEM bright-field images of the dendrites in three regions from Al–Mo alloy prepared by laser alloying and remelting processes.

the Al solid solution. On the other hand, the liquidus temperature raises and falls very rapidly during laser processing and this is responsible for the undissolved. Mo powder particles.

The subsequent laser surface remelting is applied directly to melt the surface with the materials mixed

Figure 6 (a, b) TEM bright-field image of the faceted particles from Al–Mo alloy prepared by laser alloying and remelting processes. The corresponding SAD patterns with different axes shown in: (c) [0, 1, 1]; (d) [0, 1, 3]; (e) [0, 1, 2]; and (f) [1, 1, 2].

previously by laser alloying. In this case, the alloyed elements on the surface are able to redistribute by the diffusive and convective energy transport in the molten pool. In addition, the laser beam moving direction in the subsequent laser remelting process is perpendicular to that in the previous laser alloying process. This treatment certainly plays a significant role influencing the microstructural characteristic due to the convection effects. Consequently, an refined surface is achieved through the formation of the fine and homogeneously distributed intermetallics (Fig. 2).

Five basic intermetallics have been found in the alloy: (a) Al_5Mo (r) phase displaying needle-like morphology; (b) 90° dendrites having a nearly Al_5Mo stoichiometry and a tetragonal structure; (c) the 30° dendrite having Al_5Mo stoichiometry and a monoclinic structure; (d) the faceted particles having Al_7Mo stoichiometry and a f.c.c. structure; (e) the extremely

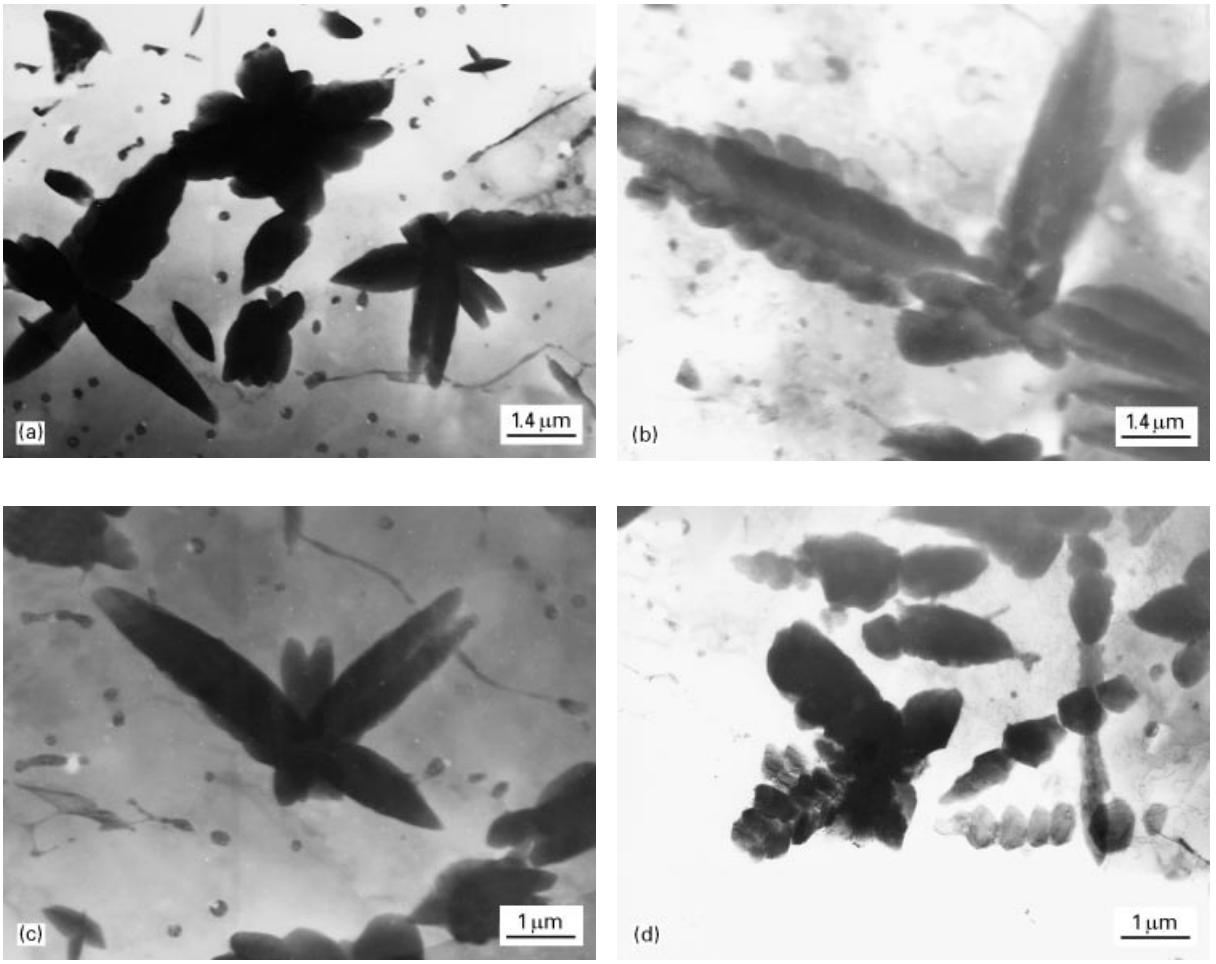

Figure 9 TEM bright-field images of the dendrites displaying a 90° angle between their primary dendrite arms.

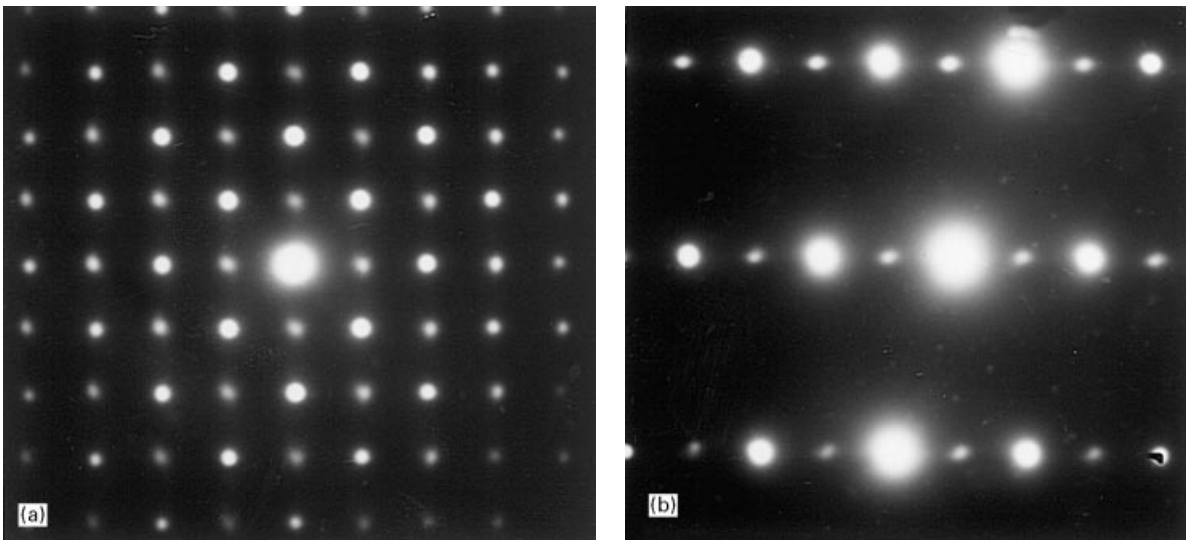

Figure 10 SAD patterns taken from the dendrites shown in Fig. 9 with zone axes: (a) [0, 0, 1]; (b) [1, 1, 2]; (c) [1, 1, −1]; and (d) [0, 1, −1].

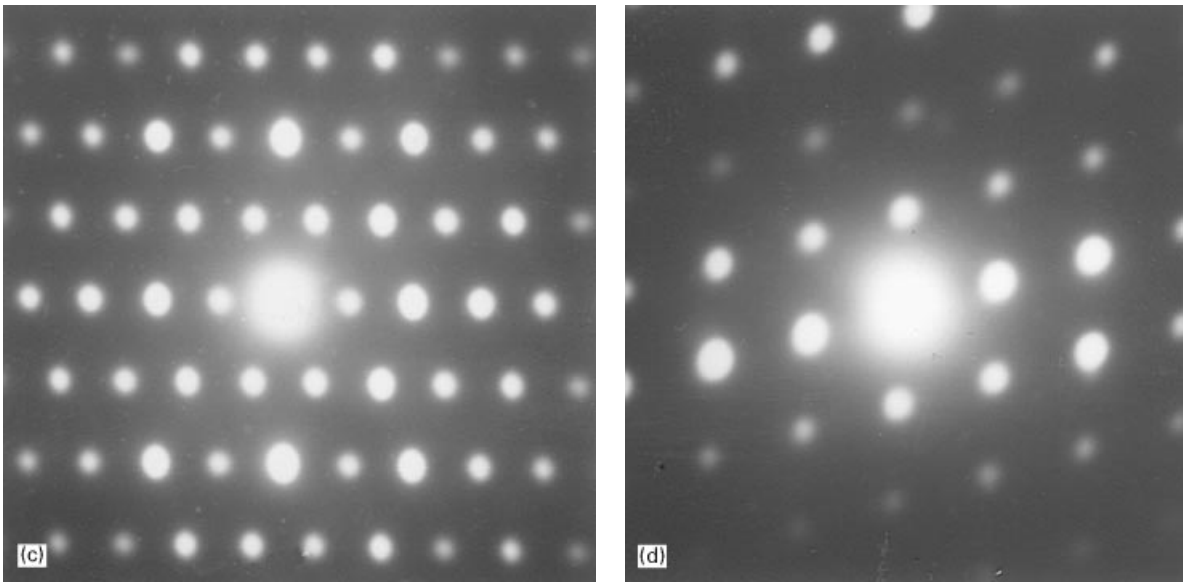

Figure 10 (*Continued*).

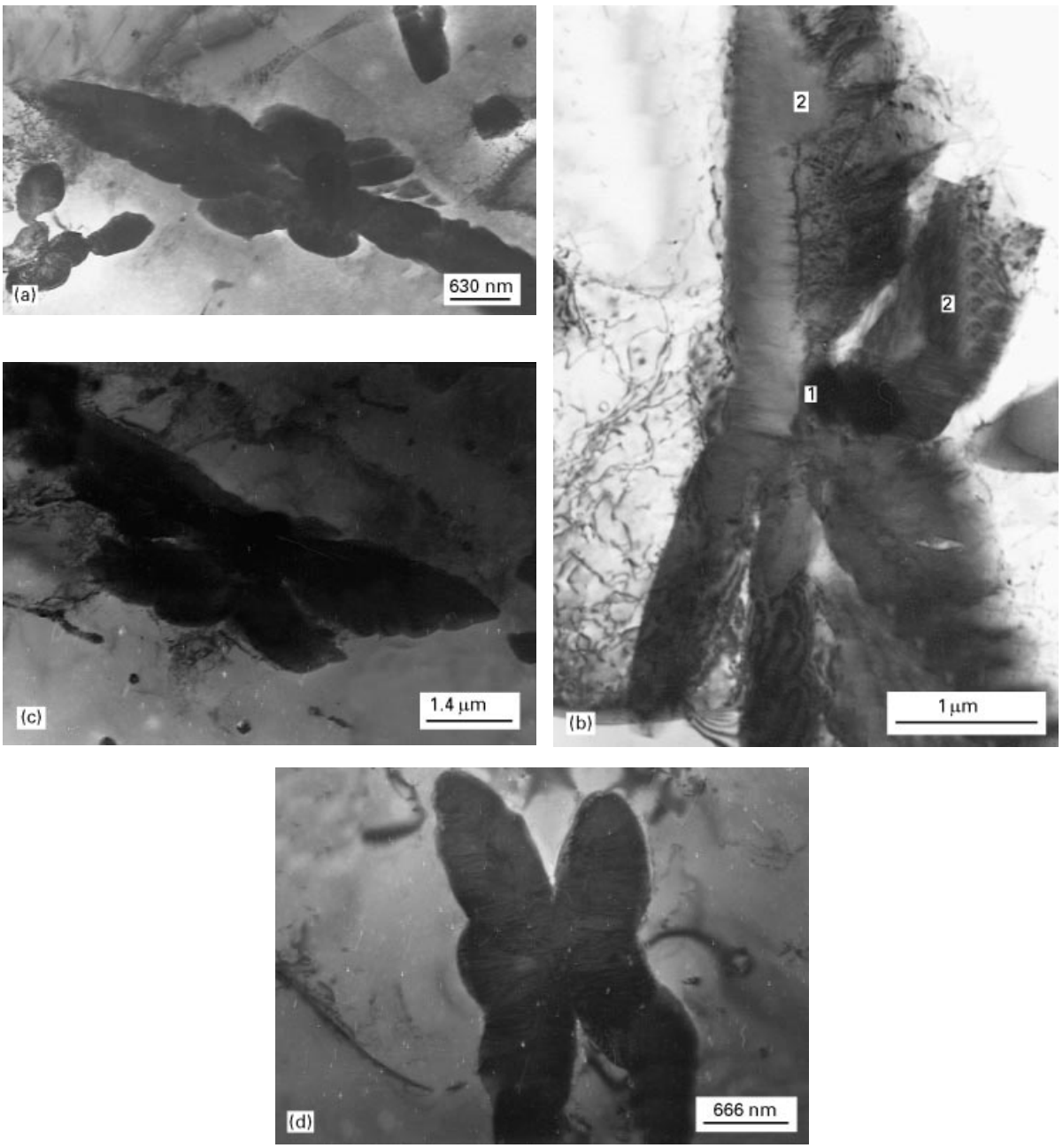

Figure 11 TEM bright-field images of the dendrite displaying a 30° or 60° angle between their primary dendrite arms.

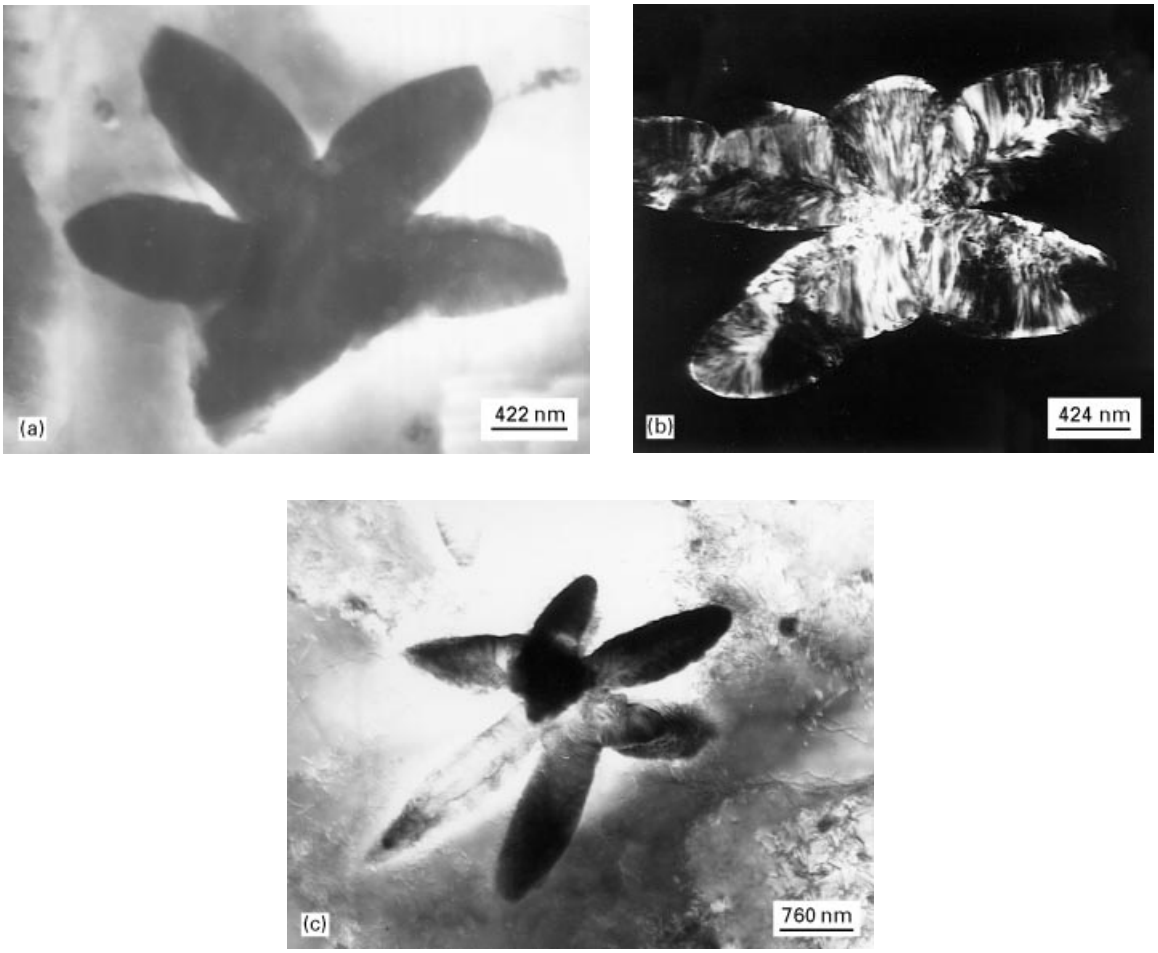

Figure 12 TEM bright-field image of the dendrites containing five dendrite arms (a) and six dendrite arms (c) with mixed 90°, 30° or 60° angles between these dendrite arms. (b) TEM dark-field image of one dendrite showing the disappearing of one dendrite arm.

fine particles having a f.c.c. structure. Among these intermetallics, only the needle-like particles are identified to be the Al_5Mo (r) phase reported by Schuster and Ipser [21]. The dendrites and the faceted particles do not match any of the known phases in Al–Mo system.

The phase diagram of the Al rich end of the Al–Mo system is still somewhat in doubt although a number of intermetallic compounds have been identified and their structure determined. The difficulty to determine the phase structure is that some of the phases contain numerous faults, for example, Al_4Mo and Al_5Mo phases [22]. Many of the intermetallics show long period superstructures which could not be attributed to one of the known phases of the Al–Mo system. It is reported that the long period superstructures are mainly derived from Al_5Mo and it was found experimentally that the Mo concentration increases with the concentration of the fault planes, suggesting that the faults correspond to missing Al plane. The faults have been observed in the dendrites (Fig. 12b) and the Al_5Mo (r) phase (Fig. 5a).

Schuster and Ipser [21] have reported that Al_5Mo (r) and Al_5Mo (h′) phases are the stacking variant of Al_5Mo (h) with the *c*-axis threefold and fivefold of the *c*-axis of Al_5Mo (h). Therefore, the periodically spaced faulted dipoles are observed in Al_5Mo (r) phase (Fig. 5a). The extra reflection (0 0 3) in Fig. 5d is believed to be the double reflection. Al_5Mo (h) is not found by TEM analysis since the TEM sample only cover the remelted layer of the alloy. The XRD results confirm the existence of the Al_5Mo (r) phase in the remelted layer.

Although the dendrite particles have a Al_5Mo stoichiometry, the SAD patterns indicate a different structure from those Al_5Mo (h, h′, r) phases. The 30° dendrites have a monoclinic structure. The 90° dendrites have a tetragonal structure. Since more 30° dendrites are found than 90° dendrites, it is believed that the 90° dendrites are metastable and will transfer to 30° dendrites. Apparently, the transformation between the 90° dendrites and 30° dendrites is only the structure transformation, i.e. tetragonal transformed to monoclinic structure. A complete structure analysis on both dendrites is still under investigation.

Al_5Mo (r) phase is the dominate phase in the alloyed layer and also in some region of the remelted layer (Fig. 1). According to the equilibrium Al-Mo

Figure 13 SAD patterns (a–c) and the corresponding computer simulation patterns (d–f) taken from the dendrites shown in Fig. 11 with zone axes: (a,d) [−1, 1, 2]: (b, e) [−1, 1, 3]: and (c,d) [−1, 1, 1].

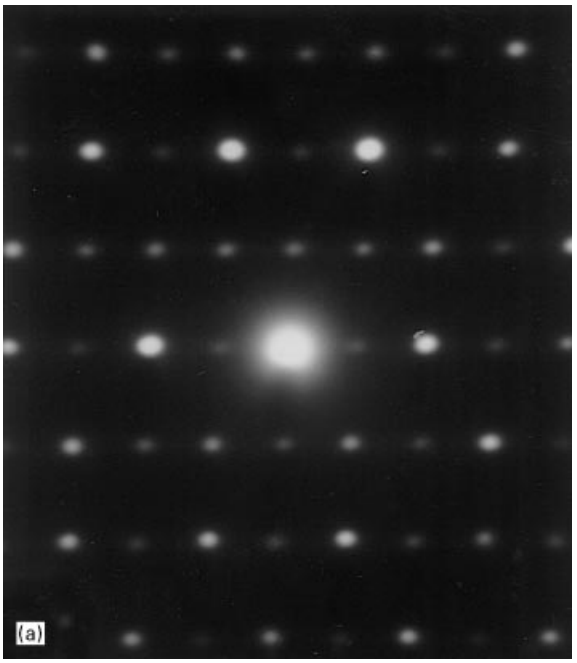
(a)

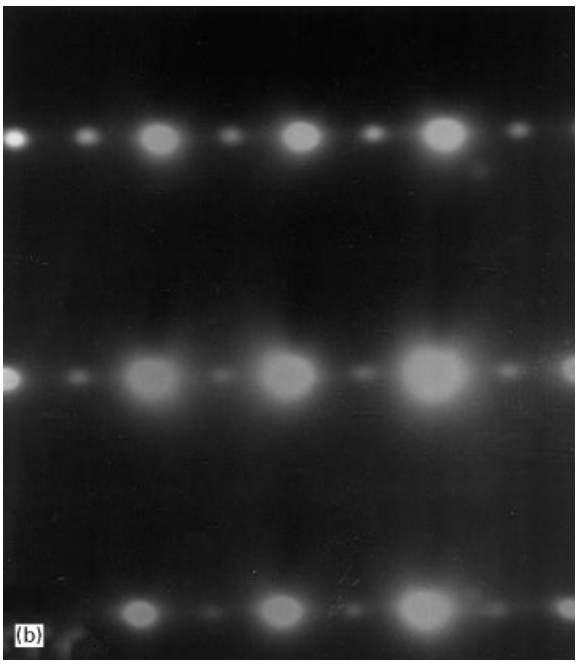
(b)

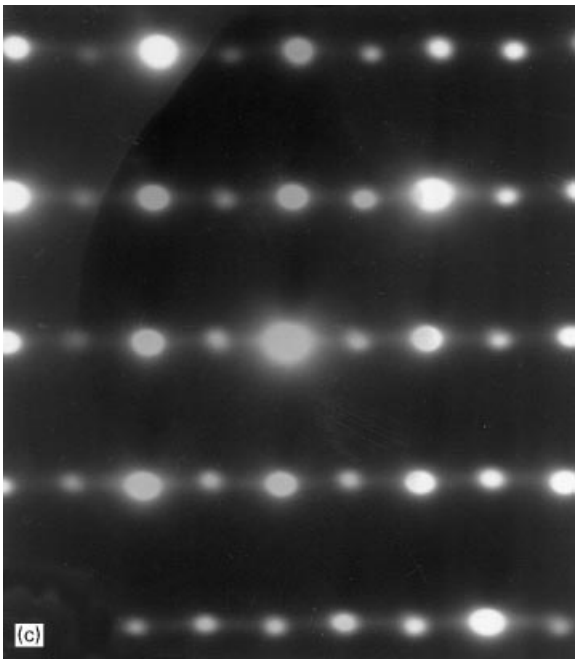
(c)

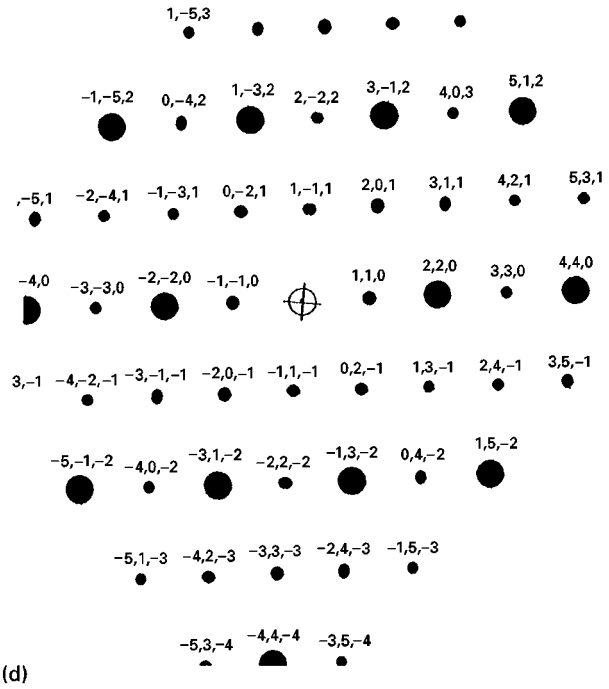
1,−5,3
−1,−5,2
0,−4,2
1,−3,2
2,−2,2
3,−1,2
4,0,3
5,1,2
,−5,1
−2,−4,1
−1,−3,1
0,−2,1
1,−1,1
2,0,1
3,1,1
4,2,1
5,3,1
−4,0
−3,−3,0
−2,−2,0
−1,−1,0
1,1,0
2,2,0
3,3,0
4,4,0
3,−1
−4,−2,−1
−3,−1,−1
−2,0,−1
−1,1,−1
0,2,−1
1,3,−1
2,4,−1
3,5,−1
−5,−1,−2
−4,0,−2
−3,1,−2
−2,2,−2
−1,3,−2
0,4,−2
1,5,−2
−5,1,−3
−4,2,−3
−3,3,−3
−2,4,−3
−1,5,−3
−5,3,−4
−4,4,−4
−3,5,−4
(d)

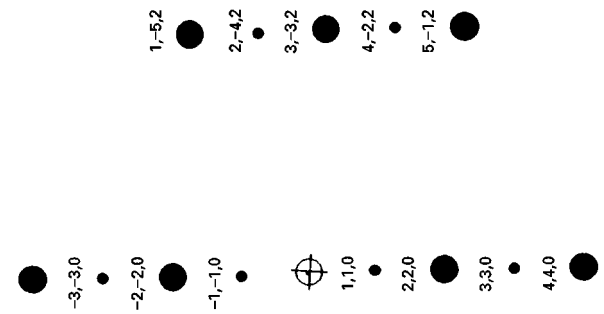
1,−5,2
2,−4,2
3,−3,2
4,−2,2
5,−1,2
−3,−3,0
−2,−2,0
−1,−1,0
1,1,0
2,2,0
3,3,0
4,4,0

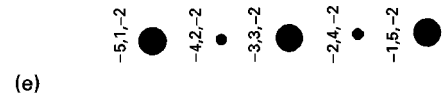
−5,1,−2
−4,2,−2
−3,3,−2
−2,4,−2
−1,5,−2
(e)

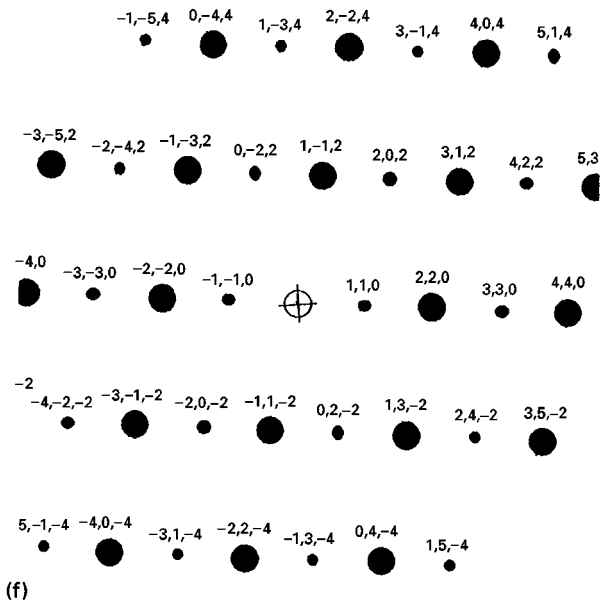
−1,−5,4
0,−4,4
1,−3,4
2,−2,4
3,−1,4
4,0,4
5,1,4
−3,−5,2
−2,−4,2
−1,−3,2
0,−2,2
1,−1,2
2,0,2
3,1,2
4,2,2
5,3
−4,0
−3,−3,0
−2,−2,0
−1,−1,0
1,1,0
2,2,0
3,3,0
4,4,0
−2
−4,−2,−2
−3,−1,−2
−2,0,−2
−1,1,−2
0,2,−2
1,3,−2
2,4,−2
3,5,−2
5,−1,−4
−4,0,−4
−3,1,−4
−2,2,−4
−1,3,−4
0,4,−4
1,5,−4
(f)

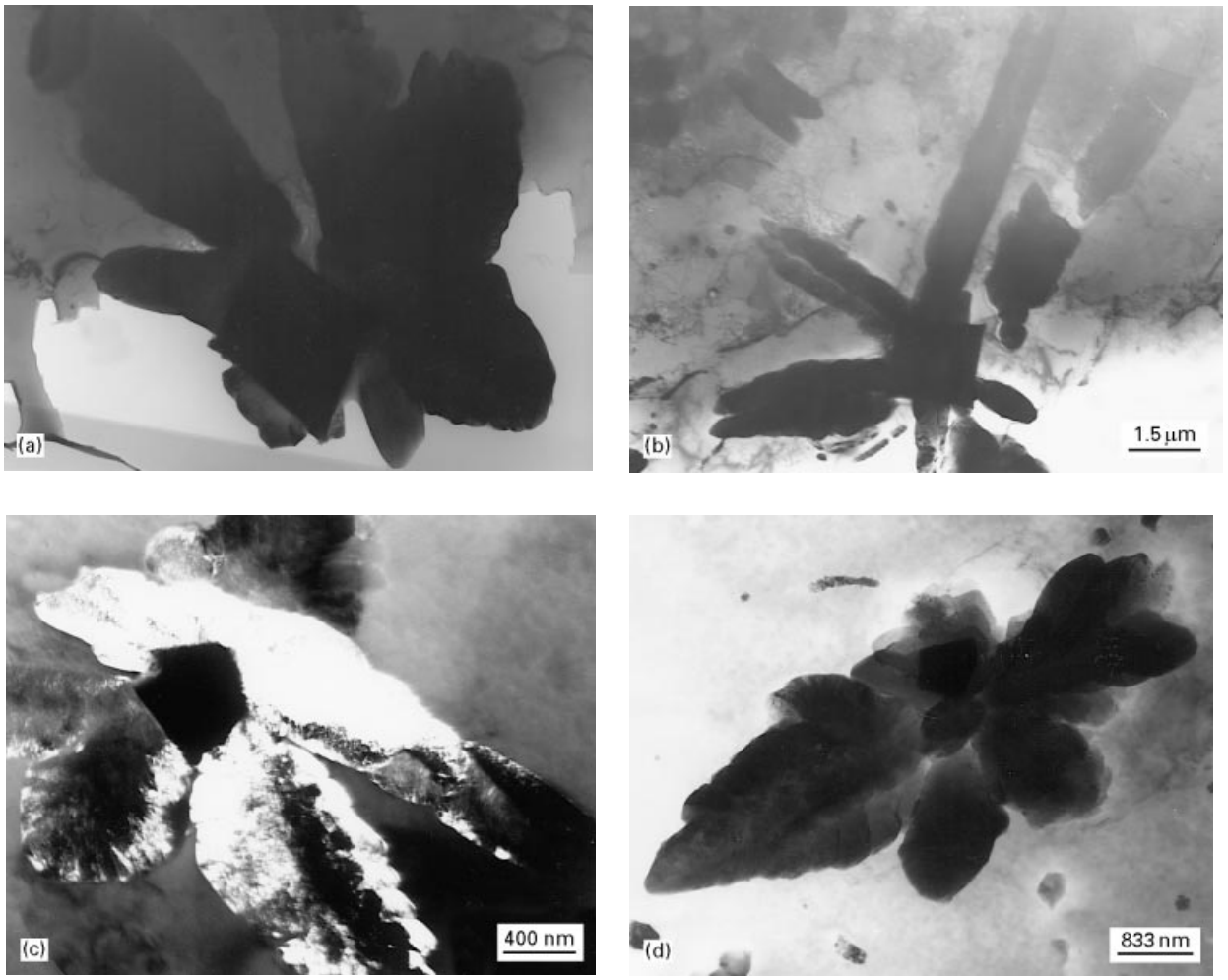

Figure 14 (a,b,d) TEM bright-field images of the dendrites showing one faceted particle located at the centre of the dendrites. (c) TEM dark-field image of the dendrite showing clearly the morphology of the centre particles.

binary diagram and the average composition of the studied alloy (1.5 at %), it is not surprising that Al_5Mo (h) phase precipitated as the primary phase in the alloyed layer and then they transferred to Al_5Mo (r). Hence, the XRD analysis indicates only the existence of the Al_5Mo (r) in the remelted layer. The transformation to Al_5Mo (h′) phase is hindered because of the high quenching rate.

The faceted particles have a Al_7Mo stoichiometry. However, the SAD analysis clearly show that these particles have a f.c.c. structure while the reported Al_7Mo have a monoclinic structure [23]. Some of these particles are located at the centre of the dendrites (Fig. 14) suggesting that they act as the nucleates for the heterogeneous nucleation of the dendrites. This kind of configuration has also been found in other systems [5].

The difference between the alloyed layer and the remelted layer is: (1) the undissolved Mo powder particles in the alloyed layer increases the local composition of the Mo after they melted during subsequent laser remelting process; (2) on the other hand, the redistribution of the Mo in short distance produces a relative homogeneous concentration within a small region; (3) the subsequent quenching rate is lower in the remelted layer due to the lower laser power used (2 kW). For (1–2), we observed that the needle-like particles dominate some area while the dendrites dominate other area (Fig. 1). For (3), we found more intermetallics precipitated in the remelted layer than in the alloyed layer.

Because the intermetallics Al_5Mo (r) have a hardness of H_V 544 under a 200 g load which is much higher than Mo (H_V 242 under a 200 g load) and Al saturated with Mo (H_V 27 under a 200 g load) [24], the homogeneous distribution of Al_5Mo (r) intermetallics and those dendrites in the remelted layer must be responsible for the improvement of the hardness on the surface of the Al alloy.

It is known that to form high melting point Al alloys, Al must be mixed with many elements. However, many elements have usually very limited solid solubility in Al alloy produced by conventional solidification techniques. The solute solubility on crystallisation has to be extended by rapid solidification techniques. Although laser alloying and remelting are mainly used for the surface structure refinement, it has been reported that by these techniques, the Cr solubility in an Al– 4.3 at % Al alloy can be extended [6]. In the present work, the Mo solubility is extended to 0.9 at % while the equilibrium solubility is 0.1 at %. Folesya *et al.* reported that about 2.5 at % Mo can be retained in solution in Al by melt spinning [16]. However, subsequent annealing of the supersaturated

alloys only leads to grain boundary precipitation of $Al_{12}Mo$ for all annealing conditions which leads to precipitation from the supersaturated solid solution. So that, despite the fact that the melt-spun solid solution is stable for many hours at temperature up to about 450°C, no useful precipitation hardening or dispersion hardening can be introduced [14]. Laser alloying and remelting are less fruitful for extending the solid solubility in the Al alloy comparing to the melt spinning techniques and by the laser surface alloying and remelting, there are always some intermetallics such as Al_5Mo appearing on the surface. However, as it was found in the present work, because these intermetallics can be refined and are homogeneously distributed in the Al solution, the hardness of the surface is largely increased [5].

5. Conclusions

Laser alloying Mo and Al powders into an Al substrate and then remelting the alloyed surface have been applied to improve the surface properties of the Al alloy. It is found that a very fine microstructure can be achieved by subsequent laser remelting on the alloyed surface. The major phase in the alloyed layer is Al_5Mo (h) and (r) phases which have a long needle-like morphologies. In the remelted layer, intermetallics with dendrite morphology formed. They are distributed homogeneously and oriented irregularly in the Al solid solution. Some faceted particles are also observed and are identified to be Al_7Mo phase with a fcc structure. The dendrites have an Al_5Mo stoichiometry and complicated structures. Al_5Mo (r) phase is found and distributed between the dendrites in the remelted layer. The formation of homogeneously distributed dendrites and Al_5Mo phase is responsible to the increasing of the hardness in the Al surface. The average Mo content in Al matrix is about 0.9 at % which is larger than that of the equilibrium solubility.

Acknowledgements

One of the authors (Y. Y. Qiu) acknowledges the support from Junta Nacional de Investigação Cientifica e Tecnolõgica Postdoctoral Scholarship.

References

1. E. W. KREUTZ, N. PIRCH and M. ROZSNOKI, "Laser treatment of materials" (B. L. Moilike DGM, 1992 (ECLAT'92)).
2. G. F. MI, S. Y. ZENG, Z. L. JIANG and Q. C. LI, *Mater. Sci. Eng.* **A179/A180** (1994) 688.
3. H. WARLIMONT, W. ZINGG and P. FURRER, *ibid.* **23** (1976) 101.
4. P. FURRER and H. WARLIMONT, *ibid.* **28** (1977) 127.
5. A. ALMEIDA, R. VILAR, R. LI, M. G. S. FERREIRA, K. G. WATKINS and W. M. STEEN, in Proceedings of ICALEO'93 (12th International Congress on Applications of Laser and Electro-Optics), edited by P. Denney, I. Myiamoto and B. L. Mordike (Laser Institute of America, Orlando, 1994) p. 903.
6. A. ALMEIDA, Y. Y. QIU and R. VILAR, *Scripta Metall.* **33** (1995) 863.
7. D. K. DAS, K. S. PRASAD and A. G. PARADKAR, *Mater. Sci. Eng.* **A174** (1994) 75.
8. E. GAFFET, J. M. PELLETIER and S. BONNET-JOBEZ, *Acta Metall.* **37** (1989) 3205.
9. L. RENAUD, F. FOUGUET, A. ELHAMDAOUI, J. P. MILLET, H. MAZILLE and J. L. CROLET, *ibid.* **38** (1990) 1574.
10. M. PIERANTONI, J. D. WAGNIERE and E. BLANK, *Mater. Sci. Eng.* **A110** (1989) L17.
11. D. K. DAS, A. G. PARADKAR and R. S. MISHRA, *Scripta Metall.* **26** (1992) 1211.
12. P. VAHILLE, S. TOSTO, J. M. PELLETIER, A. ISSA, A. B. VANNES and B. CRIQUI, *Surf. Coat. Technol.* **50** (1992) 295.
13. J. M. PELLETIER, L. RENAUD and F. FOUQUET, *Mater. Sci. Eng.* **A134** (1991) 1283.
14. C. P. CHANG and M. H. LORETTO, *ibid.* **98** (1988) 185.
15. X. D. ZHANG, Y. J. BI and M. H. LORETTO, *Acta Metall.* **41** (1993) 849.
16. A. F. POLESYA and A. I. STEPINA, *Phys. Met. Metallogr.* (Engl. Transl.) **30** (1970) 35.
17. C. P. CHANG and M. H. LORETTO, *Phil. Mag.* **57** (1988) 593.
18. *Idem., Acta Metall.* **36** (1988) 805.
19. Y. J. BI and M. H. LORETTO, *J. Rapid Solidification* **5** (1990) 163.
20. *Idem., Mater. Sci. Eng.* **A134** (1991) 1188.
21. J. C. SCHUSTER and H. IPSER, *Metall. Trans.* **22A** (1991) 1729.
22. G. VANTENDELOO, J. VAN LANDUYT and S. AMELINCKX, *Mater. Res. Bull.* **10** (1975) 941.
23. J. W. H. CLARE, *J. Inst. Met.* **89** (1960-61) 232.
24. N. TUNCA and R. W. SMITH, *Metall. Trans.* **20A** (1989) 825.

Received 7 February 1997
and accepted 5 February 1998